

Unfolding Hidden Barriers by Active Enhanced Sampling

Jing Zhang*

KLA-Tencor, AI Division

Ming Chen†

Department of Chemistry, University of California, Berkeley

(Dated: June 23, 2021)

Collective variable (CV) or order parameter based enhanced sampling algorithms have achieved great success due to their ability to efficiently explore the rough potential energy landscapes of complex systems. However, the degeneracy of microscopic configurations, originating from the orthogonal space perpendicular to the CVs, is likely to shadow “hidden barriers” and greatly reduce the efficiency of CV-based sampling. Here we demonstrate that systematic machine learning CV, through enhanced sampling, can iteratively lift such degeneracies on the fly. We introduce an active learning scheme that consists of a parametric CV learner based on deep neural network and a CV-based enhanced sampler. Our active enhanced sampling (AES) algorithm is capable of identifying the least informative regions based on a historical sample, forming a positive feedback loop between the CV learner and sampler. This approach is able to globally preserve kinetic characteristics by incrementally enhancing both sample completeness and CV quality.

Molecular dynamics (MD) simulations are an essential tool to understand the equilibria and kinetics of complex systems and processes, such as protein folding [1], drug binding [2], phase transitions [3], glass states [4, 5], etc. Sampling equilibrium states and conformational changes requires the exploration of a “rough” high-dimensional potential energy surface (PES), on which stable configurations are separated by relatively high barriers. This leads to an exponential growth of equilibration time in a MD simulation. To avoid trapping in local minima, various enhanced sampling methods have been proposed to improve the sampling efficiency [6–11]. One family of these methods including umbrella sampling [12], metadynamics [7], temperature accelerated MD [9], etc., forces the exploration of low-probability states via a biasing of the probability distribution of select degrees of freedom (DOF). Such DOFs are referred to as collective variables (CVs), which coarse-grain the high dimensional PES to a low dimensional free energy surface (FES).

An ideal set of CVs should retain the kinetic characteristics of the system [13–15] on the FES, which requires that the CVs precisely describe the low free energy regions, especially critical transition paths between minima [15]. Determining a small number of CVs to globally preserve kinetic information is quite challenging, due to the non-uniform intrinsic dimensionalities [16] and non-linear local structures of these regions [17]. One natural approach for CV selection, which has achieved some successes [18–20], seeks to empirically construct CVs based on physical intuition and structure characteristics. Other efforts have been focused on determining or training CVs through dimension reduction on simulation data [21–26]. The resulting CVs from both approaches are often kept *static* throughout the entire enhanced sampling process.

For complex chemical systems, the static form of the CVs usually leads to problematic degeneracies. In the space orthogonal to the CVs [27], potential energy barriers, a.k.a. “hidden barriers”, can separate important stable configurations. The transitions over hidden barriers that are shadowed by the chosen CVs are not observable on the FES. This phenomenon is called “orthogonal space degeneracy”. When exploring the CV space, enhanced sampling algorithms only enhance the sampling of barrier crossing on the FES, while leaving transitions over hidden barriers unaffected. Therefore, enhanced sampling algorithms rely on CV selection methods to provide a set of less-degenerate CVs. Theoretically, the set of less-degenerate CVs can be constructed given either a prior understanding of the system [19, 28, 29] or a complete sampling of the system [22–26]. Yet in practice, it is very difficult to obtain this information in a finite amount of simulation time. Hence, to break degeneracy in orthogonal space, it is vital to establish a systematic and on-the-fly approach to CV construction for enhanced sampling algorithms.

Before explaining the methodology of AES, it is worthwhile to illustrate orthogonal space degeneracy by example. For this purpose the alanine dipeptide molecule was selected. As shown in Fig. 1, two Ramachandran dihedral angles (Φ, Ψ) are usually considered as proper CVs to map all stable configurations [16] of the alanine dipeptide. Part (a) shows three major basins ($C7_{eq}$, $C5$ and $C7_{ax}$) on the FES of Φ and Ψ . As a comparison, only two minima were located when the radius of gyration (Rg) and number of hydrogen bond (NH) (commonly employed when mapping biomolecule conformations [10, 30, 31], see *SI*) were selected as CVs, see Fig. 1(b). It is clear that $C7_{eq}$ and $C7_{ax}$ are degenerate with similar Rg and NH values, which greatly reduces the sampling efficiency of $C7_{ax}$, as illustrated in Fig. 1(e). Denoting the $C7_{ax}$ basin as A , we estimate the sampling efficiency via a normalized auto-correlation

* jing.zhang@kla-tencor.com

† mingchen.chem@berkeley.edu

function $C(t) = \langle \mathbb{1}_A(\mathbf{x}(0))\mathbb{1}_A(\mathbf{x}(t)) \rangle / \langle \mathbb{1}_A^2(\mathbf{x}(0)) \rangle$, where $A = \{\mathbf{x} : 17.2^\circ \leq \Phi(\mathbf{x}) \leq 126.1^\circ\}$ and \mathbf{x} are system Cartesian coordinates. $C(t)$ measures the possibility of finding the system, with initial $C7_{ax}$ configuration, staying in A at time t . Faster decay of $C(t)$ suggests a shorter average time for the system to escape from $C7_{ax}$, and vice versa. Fig. 1(e) clearly shows that well-tempered metadynamics (WTM) [8] with Rg and NH produces a very slow decay of $C(t)$, indicating that transitions between $C7_{ax}$ and $C7_{eq}/C5$ are not enhanced due to degeneracy while applying Φ and Ψ removes the degeneracy. Thus $C(t)$ decays much faster. Unlike alanine dipeptide, in a more general scenario, constructing a small working set of such CVs is almost impossible without a thorough knowledge of the system.

Instead of well chosen CVs from prior knowledge, this work proposes Active Enhanced Sampling (AES) as a solution, which can start with arbitrary CVs and iteratively improve CV quality via active learning. Active learning is a semi-supervised learning algorithm to conductively query samples or desired outputs from the current least informative regions (CLIRs) as new learning samples. Similarly, AES introduces Stochastic Kinetic Embedding (StKE) to generate the low dimensional CV representation that preserves kinetic information and determines the CLIRs including degenerate states. Such CV representation (created by StKE) along with a FES sampler guides the MD simulation to explore these CLIRs more efficiently; on the other hand, the configurations generated by the sampler improves the learning of StKE.

The formalism of StKE is described as below. Assuming Cartesian coordinates of the system are \mathbf{x} , N_h generalized coordinates are denoted as $\mathbf{q}^h(\mathbf{x})$ and selected to characterize all slow modes. CVs are defined as $N_l < N_h$ functions of \mathbf{q}^h , i.e. $\{\mathbf{q}^l(\mathbf{q}^h(\mathbf{x}))\}$. Given a set of samples of generalized coordinates $\mathbf{s}_n^h = \mathbf{q}^h(\mathbf{x}_n) \in \mathbb{R}^{N_h}$, $n = 1, 2, \dots, N_s$ with N_s as the total number of samples, and the associated Boltzmann probability $p(\mathbf{s}_n^h)$, StKE determines a projection of $f : \mathbf{s}_n^h \in \mathbb{R}^{N_h} \rightarrow \mathbf{s}_n^l \in \mathbb{R}^{N_l}$, such that the diffusion distance [24] between each pair of datapoints is optimally retained. StKE assumes the samples are generated from an implicit diffusion process. A Markov chain is defined on $\{\mathbf{s}_n^h\}$ with an unnormalized transition matrix as $L(\mathbf{s}_i^h, \mathbf{s}_j^h) = K(\mathbf{s}_i^h, \mathbf{s}_j^h) / \sqrt{p(\mathbf{s}_i^h)p(\mathbf{s}_j^h)}$ where $K(\mathbf{s}_i^h, \mathbf{s}_j^h)$ is a Gaussian kernel describing the Brownian motion transition probability from datapoint \mathbf{s}_i^h to \mathbf{s}_j^h within a finite time step and $p(\mathbf{s}_i^h)$ is estimated via kernel density estimator. For unbiased samples $\{\mathbf{s}^h\}$ with weights $\{\omega\}$ from enhanced sampler, normalizing L generates proper transition matrix M , i.e. $M_{i,j} \equiv M(\mathbf{s}_i^h, \mathbf{s}_j^h) = \omega_j L(\mathbf{s}_i^h, \mathbf{s}_j^h) / D_i$ where $D_i = \sum_j \omega_j L(\mathbf{s}_i^h, \mathbf{s}_j^h)$ (for derivation, see SI). It has been proven that in the limit of an infinite number of samples, M will weakly converge to the generator of the diffusion process [32]. Different from several well-established dimensionality reduction methods for CVs, including diffusion map [16, 24], SGOOP [25], tICA [26], etc, which utilize low-rank ap-

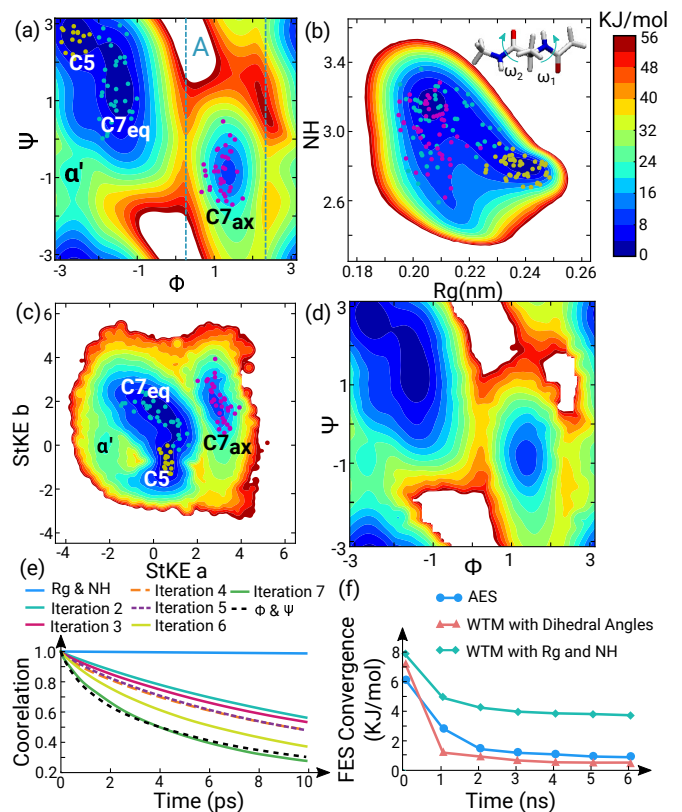


FIG. 1. FESs of alanine dipeptide (b) in gas phase with respect to (a) Ramachandran dihedral angles (Φ and Ψ), (b) Rg and NH are shown. Each FES was constructed from configurations sampled by 100ns WTMs with individual set of CVs. Four minima can be located on the (a) FES of Φ and Ψ , named as $C7_{eq}$, $C5$, $C7_{ax}$, and α' . AES was performed on this system with \mathbf{q}^h combining both Ramachandran dihedral angles and dihedral angles of amide groups (ω_1 and ω_2) (inset of (b)). After 7 iterations (6.5ns in total) of AES, all configurations are accumulated and unbiased. These unbiased configurations are mapped onto the StKE CVs trained in AES iteration 7 to generate the FES shown in part (c). Configurations from $C7_{eq}$, $C5$, and $C7_{ax}$ are scattered on all three FESs as cyan, yellow, magenta dots, respectively. Different $C(t)$ are calculated from WTM trajectories using Rg and NH, StKE CVs trained in each AES iteration, and Ramachandran dihedral angles. Each WTM was 100ns and samples for calculating $C(t)$ were collected after 50ns such that biasing potentials were well-converged. (f) FES convergence was calculated by unbiased samples from AES, WTM with Φ and Ψ , and WTM with Rg and NH. The benchmark FES is from part (a).

proximation that truncates the number of CVs at a chosen spectral gap, StKE adopts the spirit of tSNE [33] by applying Kullback-Leibler divergence to estimate the similarity of M between the higher-dimension (M^{high}) and the lower-dimension (M^{low}) for all pairs of data-

points,

$$C = \sum_i \left(\sum_j M_{i,j}^{high} \log \frac{M_{i,j}^{high}}{M_{i,j}^{low}} \right). \quad (1)$$

To ensure that StKE learns an explicit function form for the projection function f , we assume that f can be approximated by a parametric model $F(\mathbf{s}^h; W) \approx f(\mathbf{s}^h)$, where W is trainable parameters for model F . A parametrized normalized transition matrix in lower dimension defined as $\tilde{M}_{i,j}^{low}(W) \equiv M^{low}(F(\mathbf{s}_i^h; W), F(\mathbf{s}_j^h; W))$ replaces $M_{i,j}^{low}$ in Eq.(1), generating the objective function $C(W)$. Thus, W can be learned by minimizing $C(W)$ and model F can be trained via efficient stochastic gradient descent method.

As the parametric model $F(\mathbf{s}^h; W)$ has to be differentiable so that the biasing force can be evaluated in an MD simulation with enhanced sampling methods, a neural network is a practical choice for this model, e.g. multilayer perceptron (MLP). MLP consists of multiple fully-connected layers and non-linear activations to simulate the complex function form for the projection f . Since the neural network is differentiable with respect to both input and output space, this enables an estimate of $\partial f(\mathbf{s}^h)/\partial \mathbf{s}^h$ by $\partial F(\mathbf{s}^h; W)/\partial \mathbf{s}^h$, which further allows samplers to estimate biasing forces on the fly.

AES uses WTM as FES sampler, WTM fills the FES with a time-dependent biasing potential by depositing Gaussians on the fly along the simulation trajectory [7, 8], where gaussian heights in WTM decrease as the FES fills up. In the long time limit, it has been proven that the biasing potential will eventually converge to the scaled inverse FES while the CV samples display a Boltzmann distribution at higher temperature $T + \Delta T$ [8, 34], where T is the system temperature and ΔT is a parameter in WTM. Since decreasing Gaussian heights can generate a more equilibrium-like simulation trajectory, it is easier to unbiased samples to the correct ensemble distribution in WTM [35, 36].

The protocol of AES is summarized as follows:

(i) AES starts from a short WTM simulation with arbitrary CVs. The initial set of $\{\mathbf{s}^h\}$ are collected and unbiased following the method in [36] to generate sample weights $\{\omega\}$.

(ii) These samples are then resampled by enforcing a minimal pairwise distance r_c to create a sparse description in low free energy regions. Probabilities of the resampled points $\{\tilde{\mathbf{s}}^h\}$, i.e. $\{p(\tilde{\mathbf{s}}^h)\}$ are calculated as a high temperature ($T_h \geq T$) Boltzmann distribution in order to emphasize low probability regions. $\{\tilde{\mathbf{s}}^h\}$ and $\{p(\tilde{\mathbf{s}}^h)\}$ are then used to train StKE CVs \mathbf{q}^l .

(iii) $\{\mathbf{s}^h\}$ are then mapped onto the updated StKE CVs to generate $\{\mathbf{s}^l\}$ with which an initial biasing potential is generated, i.e. $V_{init}(\mathbf{q}^l(\mathbf{x})) = \frac{kT\Delta T}{T+\Delta T} \log(\sum_i w_i e^{-\|\mathbf{q}^l(\mathbf{x}) - \mathbf{s}_i^l\|^2/\sigma_{init}} + P_0) - E_0$ where k is the Boltzmann constant. P_0 and E_0 are constant such that $\min V_{init} = 0$ and $\max V_{init}$ equals the maximum

biasing potential from the last WTM simulation. This initial biasing potential is then used in next WTM with \mathbf{q}^l as CVs.

Steps (i) to (iii) forms one AES iteration. $\{\tilde{\mathbf{s}}^h\}$ and $\{p(\tilde{\mathbf{s}}^h)\}$ are accumulated through all previous iterations to generate next CVs and the whole history of $\{\mathbf{s}^h\}$ and $\{w\}$ is kept for updating V_{init} . By explicitly forming the positive feedback loop between StKE and WTM, AES incrementally improves both sample completeness and CV quality through iterations.

Two systems were used to demonstrate the effectiveness of AES: alanine dipeptide and met-enkephalin. The simulations were performed by GROMACS 5 [37] with OPLS-AA [38] force field and PLUMED 2 [39] was used for WTM simulation. In alanine dipeptide example, samples from a 100ns WTM simulation with Φ and Ψ were used to construct a benchmark FES (Fig. 1(a)) with four minima ($C7_{eq}$, $C5$, $C7_{ax}$ and α'). Considering that two additional dihedral angles ω_1 and ω_2 are also important to capture configuration-change kinetics [40], these two dihedral angles, together with Φ and Ψ , are used as \mathbf{q}^h inputs to StKE (inset of Fig. 1(b)) for generating two CVs (i.e., StKE a and b). AES started from a 500ps WTM with Rg and NH, and followed by AES iterations each with 1ns WTM. After 7 AES iterations, configurations were accumulated and unbiased, then mapped back to Φ and Ψ to generate the FES (Fig. 1(d)). This FES is highly consistent with the benchmark. All four minima are quantitatively sampled in AES with correct free energy values. Such consistency demonstrates that AES can generate Boltzmann distributed samples after unbiased. The configurations from AES were also mapped onto the StKE CVs from the last iteration, generating a FES in Fig. 1(c).

As mentioned earlier, Rg and NH lead to degeneracy between $C7_{eq}$ and $C7_{ax}$. As shown in Fig. 1(c), StKE CVs are able to completely separate samples from different clusters. StKE CVs from AES iterations were then used in WTM simulations to calculate $C(t)$. Faster decay of $C(t)$ with respect to the number of AES iterations indicates quality improvement of StKE CVs due to the increasing completeness of data samples. At AES iteration 7, $C(t)$ decays as fast as the benchmark, indicating that StKE CVs are as good as Φ and Ψ for preserving kinetic information in alanine dipeptide. We estimated FES convergence by calculating L_1 -distance per area between a test FES and the benchmark FES in Φ and Ψ space. The test FES for AES is estimated by accumulating StKE samples and mapping them back to Φ and Ψ space. As shown in Fig. 1(f), AES achieves similar FES convergence as benchmark, indicating the ability of AES to boost sampling efficiency by iteratively improving CVs. On the other side, WTM with Rg and NH fails to achieve FES convergence comparable to benchmark.

Mapping both folded and unfolded conformations of peptide is another challenging problem [41]. AES was tested on penta-peptide met-enkephalin (Fig. 2(c)) in gas phase. StKE was used to embed 10 Ramachandran di-

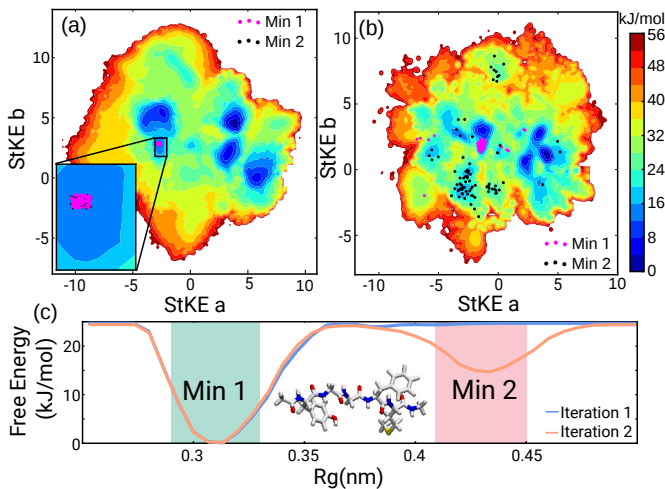


FIG. 2. Configurations sampled in AES 1st and 2nd iterations were mapped onto StKE CVs from iteration 1, generating FES shown in part (a). All the magenta and black dots lie in a neighborhood around the bottom of one minimum highlighted in part (a). The magenta dots were chosen so that their Rg values stay within the green block denoted as “Min 1” in part(c) while the black ones were selected with their Rg values in the pink block denoted as “Min 2”. Fixing the StKE CVs at this minimum, the FES along Rg is also generated with unbiased samples from iteration 1 (blue line) or with samples from both two iterations (pink line). It is clear that “Min 2” consists of new states sampled in iteration 2 with similar Rg values. In part (b), StKE CVs were trained with configurations from both iteration 1 and 2, and samples corresponding to these configurations were used to generate the FES in this part. Clearly, the structures with respect to “Min 2” were separated out, forming different minima on the FES.

hedral angles to a 2D representation. AES was initiated by a 20ns WTM with Rg, NH and backbone-heavy-atom root-mean-square deviation (RMSD) as CVs, followed by 8 AES iterations each with 100ns WTM using 2D StKE CVs and Rg. The converged 3D FES and selected stable and metastable configurations are presented in SI. In Fig. 2(a), we highlight the FES minimum where degeneracies occurred with the StKE CVs in iteration 1 due to incomplete sampling. When applying WTM with StKE CVs (from 1st iteration) and Rg, metastable configurations from degenerate states are discovered in iteration 2, as shown as the minimum 2 in Fig. 2(c). After updating StKE CVs with these metastable configurations from iteration 2, the degenerate stable states were separated as illustrated in Fig. 2(b), indicating that AES is capable of unfolding discovered hidden barriers from PES into FES that is defined by updated StKE CVs.

To evaluate the efficiency of AES, a $1\mu\text{s}$ metadynamics simulation with Rg, NH and RMSD (“regular CVs”) was performed as comparison. As demonstrated in Fig. 3(a), a faster exploration of the conformational space (represented as an increase in the resampled points) is observed for AES. Beyond 200ns, AES is able to keep a high effi-

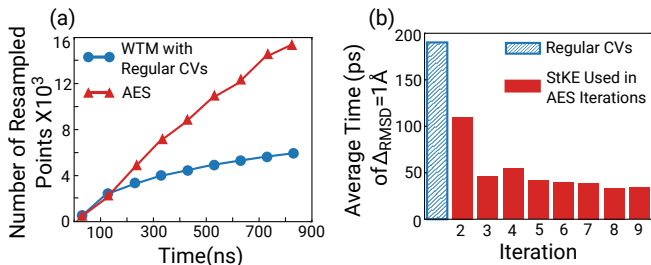


FIG. 3. The number of resampled points in 10D Ramachandran dihedral angle space v.s. total simulation time is recorded for both AES and metadynamics in part (a). This number approximates the size of sampled conformational space due to the lower bound on pairwise distances between among these points. Part (b) records the average time in which one structure changes to another with $\text{RMSD}=1\text{\AA}$. The average was taken from individual 400ns WTM with CVs used in each AES iteration. Only configurations sampled in the last 200ns were used to calculate the average, after biasing potential in WTM has filled low free energy regions in the first 200ns simulations. CVs used in iteration 1 are “regular CVs”.

ciency for discovering new configurations while the efficiency from WTM decreases. The linearly increasing of number of resampled points shows that unfolding discovered hidden barriers into FES by StKE encourages WTM to construct biasing potential more efficiently, while with *static* CVs WTM spends majority of the simulation time revisiting the stable configurations. The ability of AES to guide the enhanced sampling simulations also significantly decreases the average time needed for conformational changes since majority of “hidden barriers” are removed in AES, as shown in Fig. 3(b). In the long time limit, FES filling in WTM with regular CVs is unable to accelerate structural changes due to orthogonal space degeneracies, while StKE CVs remain faster conformational changes.

Active enhanced sampling is a framework joining CV production and sampling to unfold discovered hidden barriers into FES. In analogy to active learning, on-the-fly training StKE CVs, together with the biasing potential in WTM, guides MD simulations to sample the CLIRs. Iteratively training StKE CVs promotes the removal of orthogonal space degeneracies, boosting the sampling efficiency comparing to WTM with static and/or human intuited CVs. In alanine dipeptide example, StKE retains both intra and inter cluster structures, more importantly, the kinetic information is also preserved in StKE. In addition, minima on the FES are consistent with benchmark results, while human intuited CVs (i.e., Rg and NH) are unable to identify all minima. In met-enkephalin system, AES demonstrates its ability to remove degeneracy on the fly, leading to fast exploration of stable and metastable configurations and enhanced transitions.

Besides dihedral angles, other order parameters or those from dimension reduction algorithms, can be

adopted as \mathbf{q}^h for StKE learning. Other than WTM, enhanced sampling methods, like temperature accelerated molecular dynamics/driven adiabatic free energy dynamics [9, 10], adaptive biasing force [11], and unified free energy dynamics [42] etc., can also be married with AES. Although the present examples are calculated in

gas phase, applying AES to condensed phase simulations is straightforward.

We thank Mark E. Tuckerman, Yu Zhao and Tyler Y. Takeshita for reading the manuscript and giving suggestions. We also thank Phillip Geissler for useful discussion.

-
- [1] B. Rizzuti and V. Daggett, Arch. Biochem. and Biophys. **531**, 128 (2013).
- [2] M. De Vivo, M. Masetti, G. Bottegoni, and A. Cavalli, J. Med. Chem. **59**, 4035 (2016).
- [3] G. C. Sosso, J. Chen, S. J. Cox, M. Fitzner, P. Pedevilla, A. Zen, and A. Michaelides, Chem. Rev. **116**, 7078 (2016).
- [4] C. Massobrio, J. Du, M. Bernasconi, and P. Salmon, *Molecular Dynamics Simulations of Disordered Materials: From Network Glasses to Phase-Change Memory Alloys*, Springer Series in Materials Science (Springer International Publishing, 2015).
- [5] L. Berthier and G. Biroli, Rev. Mod. Phys. **83**, 587 (2011).
- [6] Y. Sugita and Y. Okamoto, Chem. Phys. Lett. **314**, 141 (1999).
- [7] A. Laio and M. Parrinello, Proc. Natl. Acad. Sci. U.S.A. **99**, 12562 (2002).
- [8] A. Barducci, G. Bussi, and M. Parrinello, Phys. Rev. Lett. **100**, 020603 (2008).
- [9] L. Maragliano and E. Vanden-Eijnden, Chem. Phys. Lett. **426**, 168 (2006).
- [10] J. B. Abrams and M. E. Tuckerman, J. Phys. Chem. B **112**, 15742 (2008).
- [11] E. Darve, D. Rodríguez-Gómez, and A. Pohorille, J. Chem. Phys. **128**, 144120 (2008).
- [12] G. Torrie and J. Valleau, J. Comput. Phys. **23**, 187 (1977).
- [13] R. Du, V. S. Pande, A. Y. Grosberg, T. Tanaka, and E. S. Shakhnovich, J. Chem. Phys. **108**, 334 (1998).
- [14] P. L. Geissler, C. Dellago, and D. Chandler, J. Phys. Chem. B **103**, 3706 (1999).
- [15] W. E, W. Ren, and E. Vanden-Eijnden, Chem. Phys. Lett. **413**, 242 (2005).
- [16] M. A. Rohrdanz, W. Zheng, M. Maggioni, and C. Clementi, J. Chem. Phys. **134**, 124116 (2011).
- [17] R. Hegger, A. Altis, P. H. Nguyen, and G. Stock, Phys. Rev. Lett. **98**, 028102 (2007).
- [18] H. Nymeyer, N. D. Socci, and J. N. Onuchic, Proc. Natl. Acad. Sci. U.S.A. **97**, 634 (2000).
- [19] F. Pietrucci and A. Laio, J. Chem. Theory Comput. **5**, 2197 (2009).
- [20] T.-Q. Yu and M. E. Tuckerman, Phys. Rev. Lett. **107**, 015701 (2011).
- [21] D. M. F. Van Aalten, B. L. De Groot, J. B. C. Findlay, H. J. C. Berendsen, and A. Amadei, J. Comput. Chem. **18**, 169 (1997).
- [22] P. Das, M. Moll, H. Stamati, L. E. Kaviraki, and C. Clementi, Proc. Natl. Acad. Sci. U.S.A. **103**, 9885 (2006).
- [23] M. Ceriotti, G. A. Tribello, and M. Parrinello, Proc. Natl. Acad. Sci. U.S.A. **108**, 13023 (2011).
- [24] R. R. Coifman, I. G. Kevrekidis, S. Lafon, M. Maggioni, and B. Nadler, Multiscale Modeling & Simulation **7**, 842 (2008).
- [25] P. Tiwary and B. J. Berne, Proc. Natl. Acad. Sci. U.S.A. **113**, 2839 (2016).
- [26] G. Pérez-Hernández, F. Paul, T. Giorgino, G. D. Fabritiis, and F. Noé, J. Chem. Phys. **139**, 015102 (2013).
- [27] L. Zheng, M. Chen, and W. Yang, Proc. Natl. Acad. Sci. U.S.A. **105**, 20227 (2008).
- [28] P. J. Steinhardt, D. R. Nelson, and M. Ronchetti, Phys. Rev. B **28**, 784 (1983).
- [29] F. Giberti, G. A. Tribello, and M. Parrinello, J. Chem. Theory Comput. **9**, 2526 (2013).
- [30] A. Barducci, M. Bonomi, M. K. Prakash, and M. Parrinello, Proc. Natl. Acad. Sci. U.S.A. **110**, E4708 (2013).
- [31] T.-Q. Yu, J. Lu, C. F. Abrams, and E. Vanden-Eijnden, Proc. Natl. Acad. Sci. U.S.A. **113**, 11744 (2016).
- [32] R. R. Coifman and S. Lafon, Appl. Comput. Harmon. Anal. **21**, 5 (2006).
- [33] L. van der Maaten and G. Hinton, J. Mach. Learn. Res. **9**, 2579 (2008).
- [34] J. F. Dama, M. Parrinello, and G. A. Voth, Phys. Rev. Lett. **112**, 240602 (2014).
- [35] M. Bonomi, A. Barducci, and M. Parrinello, J. Comput. Chem. **30**, 1615 (2009).
- [36] P. Tiwary and M. Parrinello, J. Phys. Chem. B **119**, 736 (2015).
- [37] M. J. Abraham, T. Murtola, R. Schulz, S. Páll, J. C. Smith, B. Hess, and E. Lindahl, SoftwareX **1–2**, 19 (2015).
- [38] G. A. Kaminski, R. A. Friesner, J. Tirado-Rives, and W. L. Jorgensen, J. Phys. Chem. B **105**, 6474 (2001).
- [39] G. A. Tribello, M. Bonomi, D. Branduardi, C. Camilloni, and G. Bussi, Comput. Phys. Commun. **185**, 604 (2014).
- [40] P. G. Bolhuis, C. Dellago, and D. Chandler, Proc. Natl. Acad. Sci. U.S.A. **97**, 5877 (2000).
- [41] M. Chen, T.-Q. Yu, and M. E. Tuckerman, Proc. Natl. Acad. Sci. U.S.A. **112**, 3235 (2015).
- [42] M. Chen, M. A. Cuendet, and M. E. Tuckerman, J. Chem. Phys. **137**, 024102 (2012).